Title

Simultaneous imaging of human cone mosaic with adaptive optics enhanced scanning laser ophthalmoscopy and high-speed transversal scanning optical coherence tomography.

Journal

Optics Letters, 33(1)

ISSN

0146-9592

Authors

Pircher, M
Zawadzki, RJ
Evans, JW
et al.

Publication Date

2008

DOI

10.1364/ol.33.000022

Peer reviewed

Simultaneous imaging of human cone mosaic with adaptive optics enhanced scanning laser ophthalmoscopy and high-speed transversal scanning optical coherence tomography

M. Pircher,[1,*] R. J. Zawadzki,[2] J. W. Evans,[2] J. S. Werner,[2] and C. K. Hitzenberger[1]

[1]*Center for Biomedical Engineering and Physics, Medical University of Vienna, Vienna, Austria*
[2]*Vision Science and Advanced Retinal Imaging Laboratory (VSRI), Department of Ophthalmology and Vision Science, University of California, Davis, Sacramento, California 95817, USA*
**Corresponding author: michael.pircher@meduniwien.ac.at*

Received August 29, 2007; revised November 9, 2007; accepted November 12, 2007;
posted November 19, 2007 (Doc. ID 87024); published December 18, 2007

We describe a novel instrument capable of acquiring, simultaneously, adaptive optics enhanced scanning laser ophthalmoscopy and optical coherence tomography (OCT) images of the human cone mosaic *in vivo*. The OCT system is based on transversal scanning of the sample with a line scan rate of 14 kHz, ~20 times faster than a previously reported instrument. We demonstrate the capability of this instrument with the measurement of the human cone spacing in perifoveal retina. © 2007 Optical Society of America

OCIS codes: 170.4500, 120.3890, 170.0110, 010.1080.

Imaging the human retina *in vivo* on a cellular level can only be achieved on a limited basis due to imperfections of the eye optics. It has been successfully demonstrated with the use of adaptive optics (AO) that aberrations introduced by the ocular media (cornea and lens) can be reduced [1], and a nearly diffraction limited transverse resolution can be achieved in retinal imaging. Confocal gating is often used to obtain depth information [2]; however, differentiating between neighboring layers of the retina requires better depth resolution. Therefore, in recent years, a combination of AO with Fourier-domain optical coherence tomography (FD-OCT) has been presented that could further enhance not only depth resolution but sensitivity as well [3,4]. With this approach, the priority scan direction is in depth, motion artifacts in the transverse direction are more likely, and small structures (e.g., the human cone mosaic) that are only observable in the en-face imaging plane might be distorted. This limitation can be reduced by imaging small areas of the retina [5]; however, this greatly limits the functionality of the instrument for clinical uses. Transversal scanning (TS) (or en-face) OCT [6] uses a different concept of image acquisition and may overcome this limitation. Another advantage of TS-OCT is the possibility of acquiring, simultaneously, scanning laser ophthalmoscope (SLO) images [7] and to dynamically shift the focus together with the coherence gate to maintain high transverse resolution throughout the imaging depth [8]. Recently, a first combination of TS-OCT with AO has been presented, however, at a rather low imaging speed [9].

In this Letter we introduce a high-speed imaging system based on TS-OCT that is capable of acquiring, simultaneously, SLO and OCT images of the human cone mosaic. The experimental setup consists of a fiber based Mach–Zehnder interferometer as shown in Fig. 1. The light that is emitted by a superluminescent diode (Superlum, Russia, $\lambda = 841$ nm, $\Delta\lambda = 51$ nm) is coupled into a single-mode-fiber beam splitter, where 20% of the light is directed into the sample arm, and 80% is directed into the reference arm. The light path in the sample arm contains the AO subsystem that is similar to a previously published instrument [10]. Additionally, the sample arm incorporates a resonant scanner (x direction) working at 14 kHz and a galvanometer scanner (y direction). Each scanner was placed at a plane that was conjugate with the pupil plane of the eye. The light power on the cornea was measured with 300 μW, which is well below the safety limits for this wavelength region. The light returning from the eye followed the same path through the AO system and was coupled back into the 80:20 fiber beam splitter. After traversing this first fiber beam splitter, the light was split by a 50:50 fiber beam splitter into two equal parts to provide the same power returning from the eye for

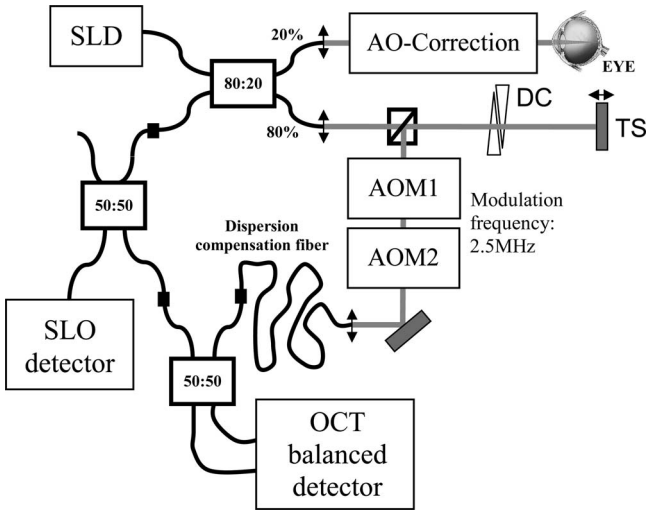

Fig. 1. Sketch of the instrument. SLD, superluminescent diode; AOM, acousto-optic modulator; TS, motorized translation stage; DC, prism for dispersion compensation.

0146-9592/08/010022-3/$15.00

the SLO and OCT channels, respectively. Note that this configuration ensures a pixel-to-pixel correspondence between both channels. The reference arm consists of a motorized translation stage for depth scanning and two acousto-optic modulators (AOMs) that generate a net carrier frequency of 2.5 MHz. Light from the sample and reference arms were recombined by the final 50:50 fiber beam splitter. The interference signal was detected by a balanced receiver, amplified, and recorded by a data acquisition board. The current configuration records SLO and OCT images, simultaneously, each consisting of ~700 ×500 pixels at a frame rate of 28 fps. This imaging speed is approximately 20 times faster than a previously reported AO equipped TS-OCT instrument [9].

To calibrate the scanning angle of our instrument we used a model eye consisting of a lens and a well-defined pattern that was placed in the focal plane of the lens. With this configuration we measured the imaged area to be ~0.75° ×0.75° on the retina. In this Letter we were interested in imaging the photoreceptors; therefore the coherence gate was shifted by only 200 μm during measurement. The total recording time was 3 s, resulting in a 3D data set with each channel consisting of 84 frames. After image acquisition, we corrected image distortion caused by the sinusoidal motion of the resonant x scanner in a software based postprocessing step. This step was not necessary for the y direction because the scanner was operated with a sawtooth voltage. The images were corrected for transverse motion using an algorithm described in [11]. To extract the signal from a specific layer [e.g., junction between the inner segments (IS) and outer segments (OS) of the photoreceptors] from the OCT 3D data set (note that the OCT imaging plane does not necessarily coincide with the plane of a retinal layer) we used the following procedure: first, we separated the frames containing the desired layer from the rest of the volumetric data. Then we searched along an A line for the maximum signal. In parallel we enhanced the signal-to-noise ratio of the SLO channel by averaging over the same number of frames used to extract the desired layer in the OCT channel.

It has been shown that a regular spacing owing to the arrangement of the photoreceptor mosaic can be observed within two OCT layers; the junction between the IS and OS of the photoreceptors and the end tips of the photoreceptors (ETPR) (or Verhoeff's membrane) [3–5,7]. Therefore, we extracted both layers from our data.

The human cones are packed most closely in the foveal center, or foveola, and the packing density decreases with increasing retinal eccentricity [12]. To demonstrate the transverse resolution of our system, Fig. 2 presents an example of images of the human cone mosaic recorded with SLO and OCT at an eccentricity of ~0.5° from the fovea. This location includes the border between a cone spacing that can be resolved with our instrument (see the left-hand side of the images) and a cone spacing that cannot. Note that due to transverse motion occurring between the recording of Figs. 2(b) and 2(c) the imaged areas are

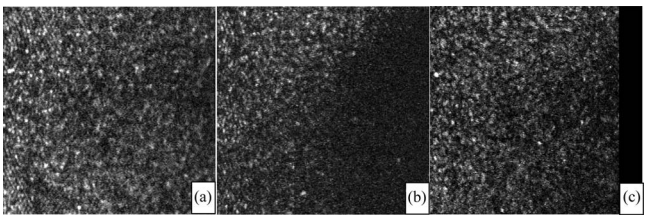

Fig. 2. Images recorded at 0.5° nasally from the fovea. (a) SLO image (average of nine frames), (b) OCT image retrieved from the IS/OS junction, (c) OCT image retrieved from the ETPR layer.

not identical. The motion correction algorithm shifts each image to compensate for the displacement; therefore a black bar is visible on the right-hand side of Fig. 2(c). It appears that the cone mosaic imaged with SLO can be observed a little closer to the fovea than the cone mosaic imaged with OCT [see Fig. 2(a) and 2(b)]. This might be caused by different speckles that are present in OCT and SLO images and by the different physical quantities measured with the two techniques (intensity in SLO versus amplitude in OCT). At this eccentricity, surprisingly, the cone mosaic retrieved from the ETPR is not clear [see Fig. 2(c)]. One possible explanation might be that a signal originating from the retinal pigment epithelium (RPE) influences the visibility of the mosaic, because at this location our depth resolution might not be sufficient to clearly separate these layers. Close to the fovea the separation between ETPR and RPE is much smaller than elsewhere. To quantitatively evaluate the cone spacing within these images we used 2D fast Fourier transformation (FFT) and custom cone-counting software [13]. Taking into account that the cone mosaic is only observable in the left-hand side of the image we calculated the 2D FFT on the left quarter of each image. Figure 3 shows the result. The regular spacing of the photoreceptors should result in the observation of Yellott's rings [14]. Instead in Figs. 3(a) and 3(b) (close to the fovea) the intensity distribution resembles a hexagonal shape, and within the image calculated from the SLO channel the intensity distribution is not uniform. It appears that six points with increased intensity forming the hexagon can be observed [see the arrows in Fig. 3(a)], which is most likely caused by the strict hexagonal packing of the photoreceptors at this eccentricity. Close to the fovea a similar observation has been made with speckle interferometry [15]. The broadening of the six points in Figs. 3(a) and 3(b) might be explained by small changes in the principal

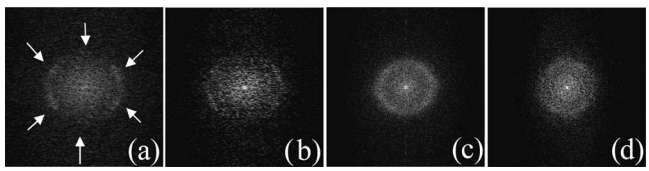

Fig. 3. Two-dimensional FFT of SLO and OCT images, respectively. (a) FFT of Fig. 2(a) (arrows point to locations with increased intensity), (b) FFT of Fig. 2(b), (c) FFT obtained from SLO image recorded at 2° eccentricity, (d) FFT obtained from OCT image (ETPR layer) recorded at 2° eccentricity.

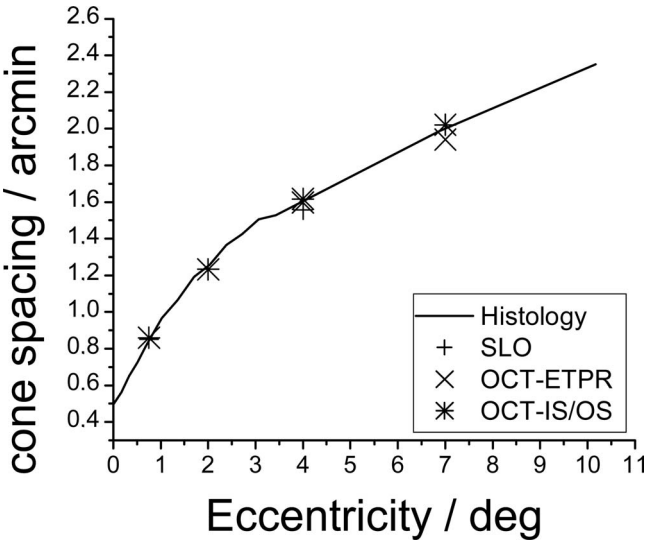

Fig. 4. Cone spacing depending on the eccentricity from the fovea. SLO cone spacing retrieved from the SLO channel, OCT-ETPR cone spacing retrieved from an imaging depth corresponding to the end tips of photoreceptors, OCT-IS/OS cone spacing retrieved from an imaging depth corresponding to the junction between the IS and OS of photoreceptors; solid curve represents values retrieved from histology [12].

axis of the hexagonal arrangement within the evaluation area.

For other eccentricities we calculated the FFT over the whole image. Figures 3(c) and 3(d) show examples of the FFT obtained from images recorded at 2° nasally from the fovea. At this location the hexagonal shape is lost, and Yellott's rings are observable, which might indicate that at this eccentricity cones are losing their hexagonal packing because of additional rods placed in between them and that the principal axis of the hexagon is changing very often within the imaging area [15]. Moreover the rings appear more homogeneous in intensity. We observed that rings retrieved from the OCT images, at all measured eccentricities, are less pronounced than that from the SLO images. Again, speckle and the different measured physical quantity might be the origin for this discrepancy. To compare our results with histology [12] we measured the radius of each ring at eight different locations and performed an average. The shape of the rings was not circular for every eccentricity; nevertheless we think that this procedure yielded mean cone spacing for each eccentricity. For the calculation from cone density to cone spacing we assumed that 1° scanning angle corresponds to 291 μm on the retina. Note that the radius of the rings corresponds to the spatial frequency of cone rows or modal frequency of the cone mosaic [16]. If we assume a hexagonal packing of the cones a multiplication by $(1/\cos 30°)$ can be used to convert the spacing between cone rows into the closest neighbor cone spacing. Figure 4 summarizes the closest neighbor cone spacing measured at different eccentricities from the fovea. The cone counting software (again assuming hexagonal packing) yielded results identical to that obtained via FFT. All results are in good agreement with histology [12].

In conclusion, we introduced a new high-speed TS-OCT system equipped with AO that is capable of imaging the human cone mosaic *in vivo* with SLO and OCT simultaneously. To the best of our knowledge, the cone mosaic has not previously been visualized this close to the fovea with OCT. The cone spacing could be measured from SLO and OCT images at different eccentricities from the fovea.

The authors thank B. Xue for performing the cone counting. Financial support from the National Eye Institute (grant EY 014743) and the Austrian Science Fund (FWF grant P16776-N02) is gratefully acknowledged.

References

1. J. Z. Liang, D. R. Williams, and D. T. Miller, J. Opt. Soc. Am. A **14**, 2884 (1997).
2. F. Romero-Borja, K. Venkateswaran, A. Roorda, and T. Hebert, Appl. Opt. **44**, 4032 (2005).
3. Y. Zhang, J. Rha, R. S. Jonnal, and D. T. Miller, Opt. Express **13**, 4792 (2005).
4. R. J. Zawadzki, S. M. Jones, S. S. Olivier, M. Zhao, B. A. Bower, J. A. Izatt, S. Choi, S. Laut, and J. S. Werner, Opt. Express **13**, 8532 (2005).
5. Y. Zhang, B. Cense, J. Rha, R. S. Jonnal, W. Gao, R. J. Zawadzki, J. S. Werner, S. M. Jones, S. S. Olivier, and D. T. Miller, Opt. Express **14**, 4380 (2006).
6. A. G. Podoleanu, G. M. Dobre, and D. A. Jackson, Opt. Lett. **23**, 147 (1998).
7. M. Pircher, B. Baumann, E. Götzinger, and C. K. Hitzenberger, Opt. Lett. **31**, 1821 (2006).
8. M. Pircher, E. Götzinger, and C. K. Hitzenberger, J. Biomed. Opt. **11**, 054013 (2006).
9. D. Merino, C. Dainty, A. Bradu, and A. G. Podoleanu, Opt. Express **14**, 3345 (2006).
10. R. J. Zawadzki, S. Choi, S. M. Jones, S. S. Olivier, and J. S. Werner, J. Opt. Soc. Am. A **24**, 1373 (2007).
11. P. Thevenaz, U. E. Ruttimann, and M. Unser, IEEE Trans. Image Process. **7**, 7 (1998).
12. C. A. Curcio, K. R. Sloan, R. E. Kalina, and A. E. Hendrickson, J. Comp. Neurol. **292**, 497 (1990).
13. B. Xue, S. S. Choi, N. Doble, and J. S. Werner, J. Opt. Soc. Am. A **24**, 1364 (2007).
14. J. I. Yellott, Jr., Vision Res. **22**, 1205 (1982).
15. S. Marcos and R. Navarro, J. Opt. Soc. Am. A **13**, 2329 (1996).
16. N. J. Coletta and D. R. Williams, J. Opt. Soc. Am. A **4**, 1503 (1987).